Beyond: Undergraduate Research Journal

Volume 1 Article 1

January 2016

Breakdown of ITCZ-like PV Patterns

Ajay Raghavendra
Embry-Riddle Aeronautical University - Daytona Beach, raghavea@my.erau.edu

Thomas A. Guinn
Embry-Riddle Aeronautical University - Daytona Beach, guinnt@erau.edu

Breakdown of ITCZ-like PV Patterns

Cover Page Footnote

We would like to thank The Office of Undergraduate Research (IGNITE), Embry-Riddle Aeronautical University for funding this research project.

UNDERGRADUATE RESEARCH JOURNAL
Beyond

Breakdown of ITCZ-like PV Patterns

Ajay Raghavendra and Thomas A. Guinn

Abstract

This study uses a shallow-water, normal-mode spectral model to examine the non-linear potential vorticity (PV) dynamics of the break¬down of both infinite an finite-length initial vorticity strips, simulating the inter-tropical convergence zone (ITCZ) found near the tropical eastern Pacific region. Irregularities in convection and diabatic heating are simulated using uniformly and randomly spaced pockets of enhanced vorticity as well as mass sinks embedded in otherwise uniform vorticity strips. Since the absolute vorticity divided by the fluid depth is materially conserved in the shallow water framework, analogies are drawn to the evolution of Ertel's PV in a stratified fluid. Results indicate the spacing of vorticity pockets had a greater influence on the evolution of PV than did broadband perturbations of the vorticity strip boundaries; however, all results were consistent with linear stability theory. Finite length initial vorticity strips of uniform width had a greater tendency to break down into two PV pools while finite strips of non-uniform width did not. This may suggest the breakdown of elongated areas of PV into two circulation centers is more likely when ITCZ convection patterns are more uniform in width.

Introduction

The Inter-Tropical Convergence Zone (ITCZ) is a zonal belt of intense convection, responsible for the genesis of over 80 percent of all tropical cyclones (Gray, 1979). This elongated band of convection is often observed to undulate and breakdown into smaller disturbances forming tropical cyclones (TCs) as seen in Fig. 1. Because the ITCZ is a region of intense diabatic heating and shear, it results in a maximum of Ertel's potential vorticity (PV), thus meeting Rayleigh's necessary condition for barotropic instability (Rayleigh, 1945; Guinn and Schubert, 1993). The dynamics associated with the breakdown of idealized ITCZ-like PV patterns have been previously investigated in numerous barotropic studies (*e.g.*, Guinn and Schubert, 1993; Neito-Ferreira and Schubert, 1997) as well as full physical model studies (*e.g.*, Wang and Magnusdottir, 2005). This paper expands the previous barotropic studies by introducing irregularities in the PV pattern representing observed irregularities in convective activity within the ITCZ as frequently occurs in the eastern tropical Pacific ocean as seen in Fig. 2. In addition, the paper investigates the effects of asymmetry in shape on the evolution of PV strips of finite length, again representing ITCZ-like structures. While the barotropic nature of the model is incapable of capturing all the moist dynamics of tropical weather systems, it does capture many of the fundamental dry dynamics. Lastly, the study also invests in

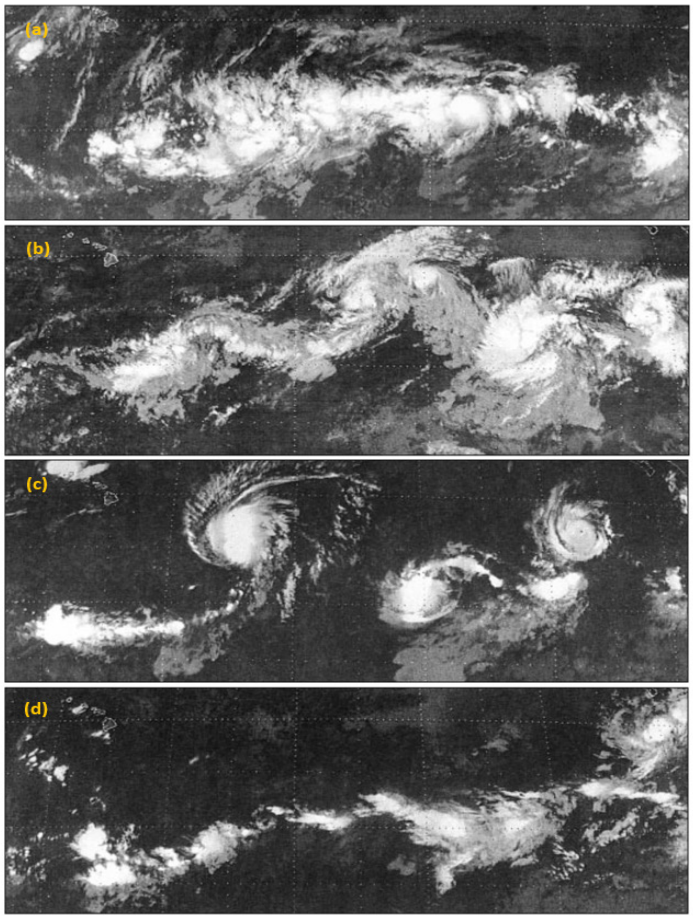

Figure 1. GOES IR images at 1646 UTC on (a) 26 July, (b) 28 July, (c) 3 August, and (d) 12 August 1988 showing a case of ITCZ breakdown (from Nieto-Ferreira and Schubert, 1997)

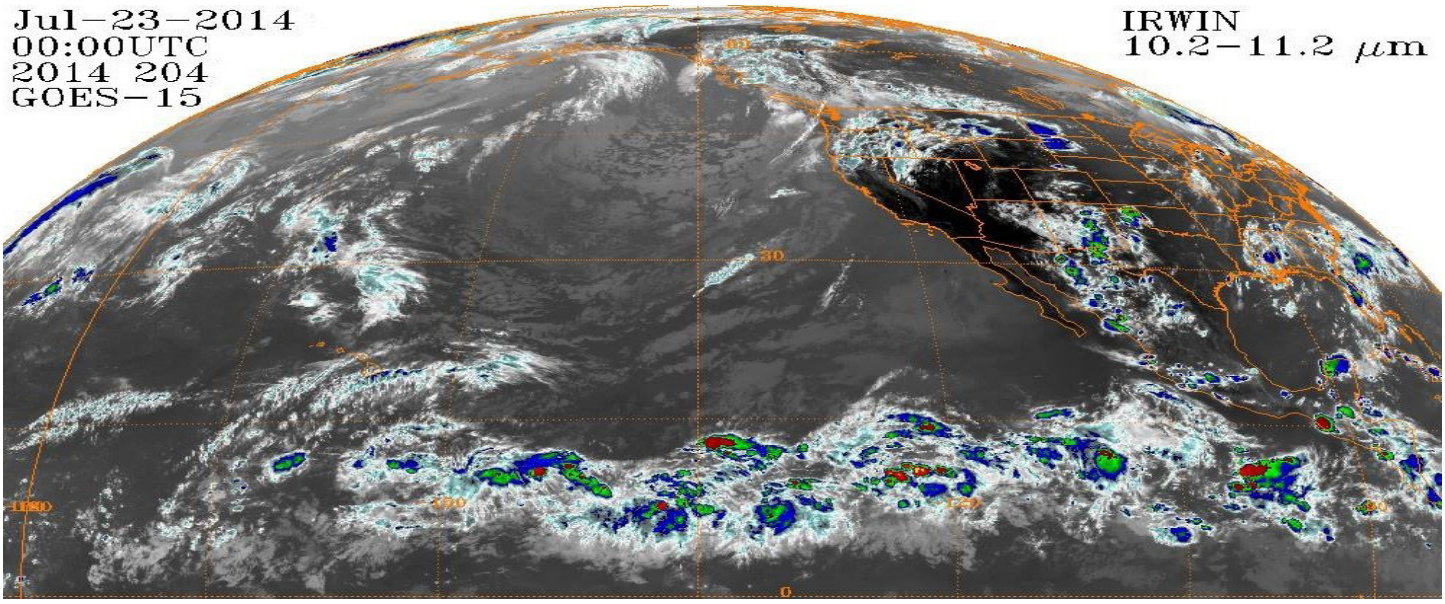

Figure 2. A GOES 15 IR image of the ITCZ. The bright colors are indicative of non-uniform convection along the ITCZ.

developing a relatively simple numerical model for use as an educational tool at the advanced undergraduate or junior graduate level.

This paper is organized as follows. We first describe the shallow water equations (SWEs) and the numerical aspects of the model, to include a description of the mass sink procedure used to represent irregularities in convective activity within the ITCZ. Next we discuss the basic initial conditions common to all six simulations presented in this paper as well as the modifications to the basic conditions that make each simulation unique. We then compare the results from each of the solutions and discuss the significance of each. Finally, we summarize the model results and offer concluding remarks regarding the model's potential use for educational purposes.

Equations and Model Background

A normal–mode spectral model was developed to solve the SWE-s in Cartesian coordinates on an *f*-plane (10° latitude was chosen for this study given the climatological persistence of the ITCZ north of the equator, (*e.g.*, S. G. H. Philander et al., 1996) using a doubly periodic domain $0 \le x \le L_x$, $0 \le y \le L_y$, where L_x and L_y represent the length and width of the model domain, respectively.

$$\frac{\partial u}{\partial t} - \left(f + \frac{\partial v}{\partial x} - \frac{\partial u}{\partial y} \right) v + \frac{\partial}{\partial x}\left[gh + \frac{1}{2}\left(u^2 + v^2\right) \right] = k\nabla^2 u \tag{1}$$

$$\frac{\partial v}{\partial t} - \left(f + \frac{\partial v}{\partial x} - \frac{\partial u}{\partial y} \right) u + \frac{\partial}{\partial y}\left[gh + \frac{1}{2}\left(u^2 + v^2\right) \right] = k\nabla^2 v \tag{2}$$

$$\frac{\partial h}{\partial t} + \frac{\partial (uh)}{\partial x} + \frac{\partial (vh)}{\partial y} = S + k\nabla^2 h \tag{3}$$

In equations (1)-(3), u and v represent the zonal and meridional components of the velocity vector, respectively, g the acceleration due to gravity, f the Coriolis parameter (a constant), h the fluid depth, S the effects of convective heating or cooling (mass sinks or sources) and k is the diffusion constant. While the planetary vorticity changes rapidly near 10°N (or S), the undulations and subsequent disturbances do not deviate significantly from their original latitude so the *f*-plane approximation is reasonable for thin strips of 300-400km (±2° latitude either side of center). However, this approximation is less valid for the finite disturbance cases as will be noted later.

Similar to Guinn (1992) and Guinn and Schubert (1993), we used the normal-mode method to solve equations (1)-(3). All simulations were conducted on a 6,400km × 6,400km domain with 512 × 512 collocation points. Time integration was performed using a fourth-order Adams-Bashforth-Moulton predictor-corrector scheme, and the total simulation length for all simulations was 120hrs using 60s time step.

To prevent aliasing of quadratically non-linear terms, we retained only 170 waves in the Fourier transform resulting in an effective horizontal resolution of approximately 37km. To reduce spectral blocking, we

included ordinary diffusion (*i.e.* $k\nabla^2 u$, $k\nabla^2 v$, and $k\nabla^2 h$ on the right hand side of equations (1) – (3). Similar to Schubert, et al. (1999) we chose a diffusion constant of 100 m^2s^{-1}, resulting in waves with total wavenumber 170 e-folding approximately every 53 minutes.

To simulate the effects of convection on the PV field, we introduced a mass sink in the mass continuity equation (3). To see the relationship of convection to mass sink, consider the following. In the shallow water framework, PV is given as:

$$PV = \frac{(\zeta + f)}{h} H \tag{4}$$

where ζ is the relative vorticity, f is the Coriolis parameter, h is the fluid depth, and H is the undisturbed fluid depth (a constant). In the absence of friction, PV is a materially conserved quantity. In the absence of frictional effects and mass sources or sinks, this quantity is materially conserved. In comparison, consider Ertel's PV, which is defined as:

$$PV = \frac{1}{\rho}(\zeta + f)\frac{\partial \theta}{\partial z} \tag{5}$$

where ρ is the density of the fluid, ζ is the relative vorticity, and θ is the potential temperature. Ertel's PV can be thought of as the absolute vorticity divided by the height difference between two θ-surfaces. In the real atmosphere, convection results in latent heat of condensation (*i.e.*, diabatic heating), which increases the vertical θ gradient, resulting in smaller distances between θ surfaces, therefore increasing the PV. In the shallow water framework, this is closely analogous to shallower fluid depth. Therefore, we can simulate the effects of diabatic heating due to convection by introducing a mass sink that locally decreases the mean fluid depth, therefore increasing the PV.

Initial Conditions

We created four variations of infinite strips of enhanced vorticity aligned in the longitudinal direction plus two finite strips (six cases total) to simulate various initial structures of the ITCZ. However, because sharp discontinuities on the edges of the initial strips would result in significant model noise due to Gibbs phenomena (*e.g.*, Mattuck et al. 2011), we instead specify our initial disturbances (as well as mass sinks) using smooth, piecewise continuous functions. Following Shubert et.al (1999), we chose a Hermite polynomial of the form $P(s)=1-3s^2+2s$ where $s \in \{0,1\}$ to smoothly transition the vorticity patterns from their maximum value near the edge of the strip (*i.e.*, $s=0$), to zero over a specified distance (*i.e.*, to $s=1$). The shape of $P(s)$ is shown in Fig. 3. Note that we also used this technique to smoothly reduce the mass sink from the region of maximum heating to zero over a specified distance in experiments where a mass sink was used (Figs. 4 and 5). Next, using the specified initial vorticity field, we extracted the initial wind and mass fields by applying the non-linear balance equation (*e.g.*, Guinn and Schubert, 1993 and DeMaria and Schubert, 1984; for a detailed explanation see Thelwell, 2011).

Mathematically, we can describe the initial vorticity field in the following manner. We first define the distance from the center of the vorticity strip at which the vorticity starts to decrease (d_s) from its central value of ζ_o as well as the distance at which the vorticity decreases to zero (d_e). We next define the normalized distance parameter (s) as:

$$s(d) = \frac{d - de}{ds - de} \tag{6}$$

which has the desired range between 0 and 1 for use with the Hermite polynomial. Using this, our shape function for our vorticity strip becomes:

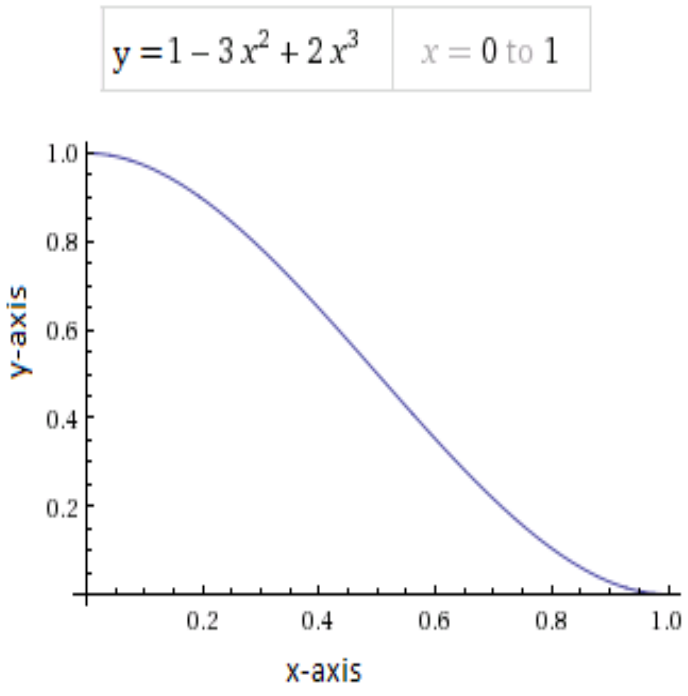

Figure 3. Plot of the cubic Hermite polynomial $P(x)=1-3x^2+2x^3$. Note that the slope, $dp(x)/dx = 0$ at $x=0$ and 1.

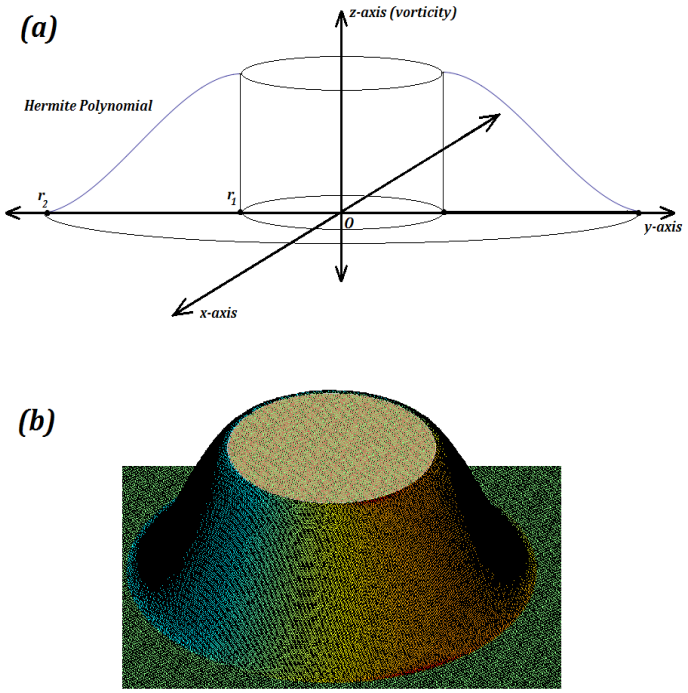

Figure 4. Visualizing a pocket of vorticity in Case 2 and 3 of this section. (a) A sketch of the vortex pocket that consists of concentric

$$\zeta(d) = \begin{cases} \zeta_o & \text{for } d < d_s \\ \zeta_o \; Hr(s(d)) & \text{for } d_s \le d \le d_e \\ 0 & \text{for } d < d_e \end{cases} \tag{7}$$

Since the spectral model is periodic in both x and y, the net circulation must be zero, or it would violate periodicity (*i.e.*, winds at opposing boundaries would not be identical). This requires the domain-averaged vorticity be zero. We can accomplish this in spectral space simply by creating the initial vorticity field then zeroing the spectral coefficients corresponding to the mean (*i.e.*, wavenumbers zero in both x and y). This introduces a weakly negative background vorticity field, which is minimized by using a larger than necessary model domain.

Case 1: Infinite Strip

For our initial case we chose a 400km wide infinite (in longitude) strip of vorticity, where the vorticity decreases (in latitude) over a distance of 100km starting 100km either side to the strips center. Specifically, starting at the center of the strip and moving perpendicular to the strip, d_s = 100km and d_e = 200km for both sides of the

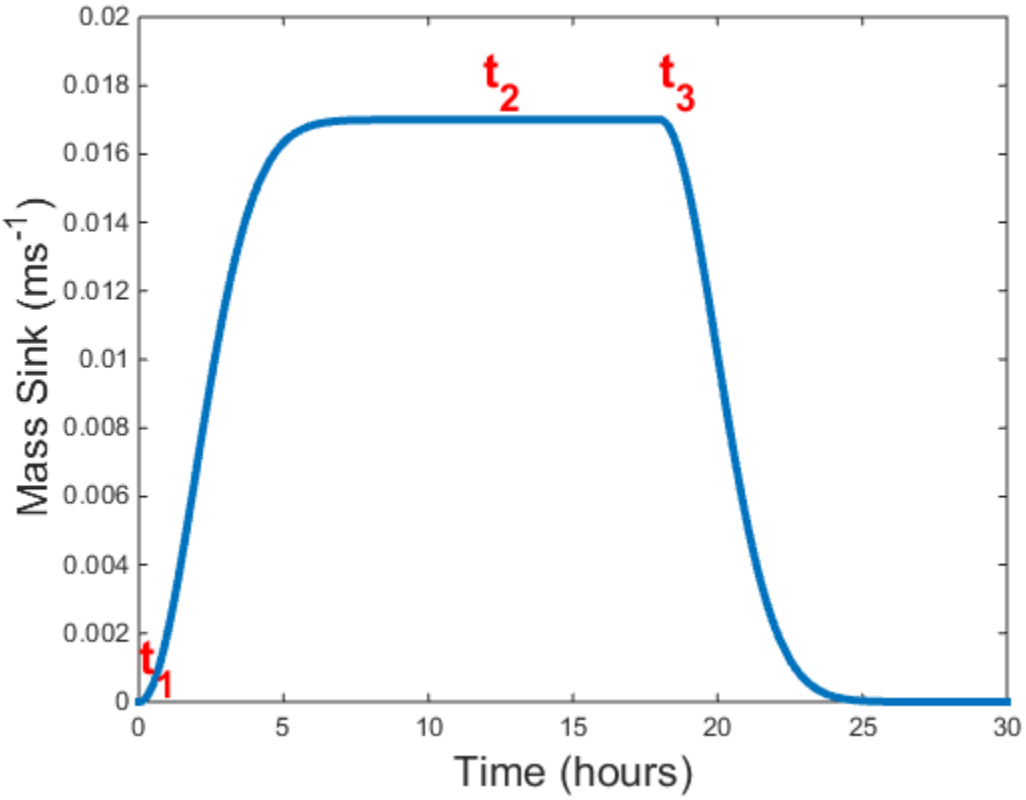

Figure 5. Time variation of the heating function for Case 4

strip. The inner 200 km wide region is a strip of uniform vorticity of value 7.5×10^{-5} s^{-1}. The results from this simple case serves as a verification for the proper function of the model and provides a foundation for all other comparisons. To accelerate the breakdown of the vortex pattern as well as better replicate the non-smooth nature of ITCZ shapes, we added a random wave number 16 broadband perturbation (*e.g.*, Schubert et.al, 1999) with a magnitude of 0.3 percent of the maximum vorticity within the strop.

Case 2: Infinite Strip with Uniformly Spaced Perturbations

Case 2 is a slight modification of case 1. Here the vorticity strip is similar in shape size and shape; however, we added 10 circular shaped vorticity perturbations that were $1.7\times10^{-5}s^{-1}$ greater that the core value of 7.4×10^{-5} s^{-1}. We decreased the core value of vorticity slightly from case 1 to maintain a similar value for the area-averaged vorticity. For the circular perturbations, we chose the inner radius of the circular region to be 40km in which the perturbation value equaled $1.7\times10^{-5}s^{-1}$. Then, in a manner similar to the infinite strip of case 1, we used a Hermite polynomial to decrease the vorticity perturbation to zero over an additional 40km.

Case 3: Infinite Strip with Randomly Spaced Perturbations

Case 3 is identical to case 2 except, the ten circular regions of perturbation vorticity are spaced in both *x* and *y* with random offsets of ±25km in *y* and ±200km in *x*. In addition, we added a ±10% random variation in the magnitude of the individual perturbation vorticity regions.

Case 4: Infinite Strip with Random Spaced Pockets of Convection

Case 4 is identical to case 1 except, there was no broadband perturbation. Instead, we added ten randomly spaced circular mass sinks positioned along the center of the strip. The seed of the random number generator was kept the same as in case 3 such that the positions of the mass sinks were identical to the previous case. The individual mass sinks each had a radius of 40km and used a Hermite polynomial used to decrease the magnitude of the sink over an additional 40km. For the heating shape function, $Q(x,y)$, we followed the same format as the shape of the vorticity pockets in case 3 and as shown in Fig. 4. For the temporal portion of the heating function, we used an exponential growth function for turning on the heating with and exponential decay function for turning off the heating. We used the same non-dimensional steepness parameter, α ($10^{-8}s^{-1}$), for both the growth and decay of the heating function. We provide a depiction of the temporal function in Fig. 5. Mathematically we used the below function to achieve the desired heating:

$$S(x,y,t)=\begin{cases} Q(x,y)[1-e^{-\alpha(t-t_2)^2}] & t_1\le t\le t_2 \\ Q(x,y) & t_2<t\le t_3 \\ Q(x,y)e^{-\alpha(t-t_3)^2} & t>t_3 \end{cases} \quad (8)$$

where, t_1,t_2, and t_3 represent the time at which the sink was turned on, maintained at a steady state, and started to decrease, respectively. At peak value, the heating function drained fluid at the rate of $0.017ms^{-1}$ to simulate a heating rate of approximately 10K per day (Guinn, 1992). In this simulation, we started the heating function at 0hrs and it achieved its peak value 12hrs into the simulation. The function maintained peak heating for 6hrs and then slowly decreased to zero over an additional 12hrs using the same steepness parameter. The heating function was therefore active for a total of 30hrs or 25 percent of the total model simulation time.

Case 5: Unsymmetrical, Finite-Length Strip

In this experiment, we chose to modify the work of Vaughan and Guinn (2013), where they examined the evolution of a symmetric, "Twinkie"-shaped finite strip of vorticity, representing a finite portion of the ITCZ. Our goal was to examine the effect of shape asymmetry in the evolution of these initial PV fields. Our motivation stemmed from the climatological persistence of similarly shaped convective patterns associated with the ITCZ in the tropical eastern Pacific (*e.g.* Waliser and Gautier, 1993 and Salby, 1991). The time lapse diagrams in Fig. 6 provide an example of the reoccurring ITCZ pattern unique to the eastern Pacific region.

Mathematically, the asymmetric or lopsided "Twinkie"-shape can be described as the resulting perimeter of two circles of radius $r_1$and r_2 separated by a distance d (measured center to center) and connected by two exterior tangent lines as shown is Fig. 7. For our specific case, we chose circles of radii 500km and 100km, separated by a distance of 2,800km. Similar to the previous initial conditions, we then used the same Hermite polynomial to reduce the vorticity from a peak value of 5.85×10^{-5} s^{-1} to zero over a distance of 100 km

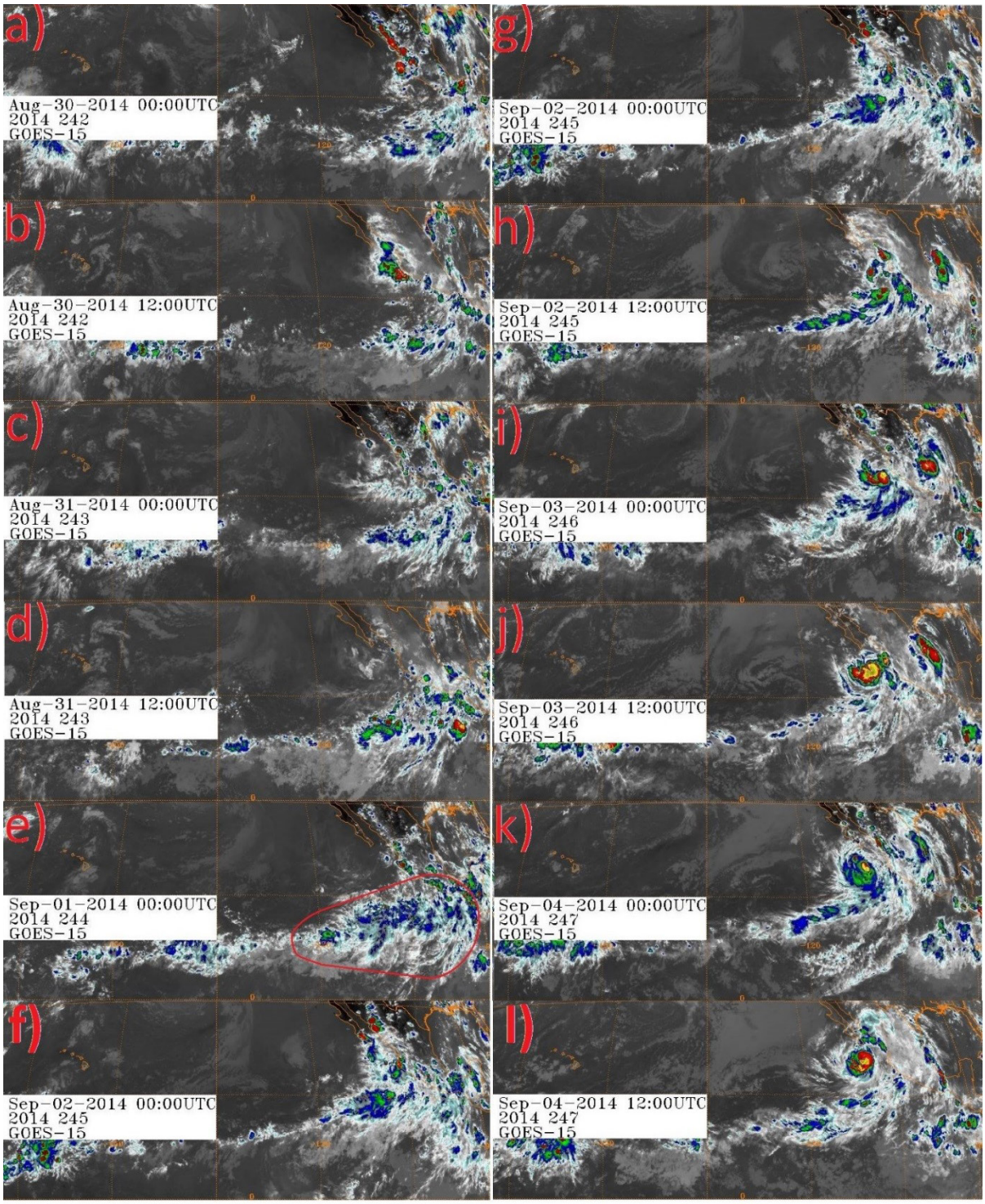

Figure 6. A GOES-15 IR time lapse of an ITCZ breakdown in the eastern Pacific occurring between 30 Aug and 4 Sep 2014.

at the outer perimeter.

Case 6: Symmetrical, Finite-Length Strip

Case 6 is a finite, symmetric "Twinkie"-shaped strip of vorticity similar to Vaughan and Guinn (2013). We chose this case for comparison with the Unsymmetrical case. This case helps in making a comparison to case 5. We again chose a size such that the total area of the strip as well as the area-averaged vorticity values were similar to case 5.

Results and Discussion

The evolution and breakdown of the four infinite strips showed only subtle differences between the individual cases, while the breakdown of the finite strips differed significantly from one other. We present the results of these six cases in this section. Fig. 8 – 13 show the time evolution of PV field at 0, 24, 48, 72, 96 and 120 hrs for

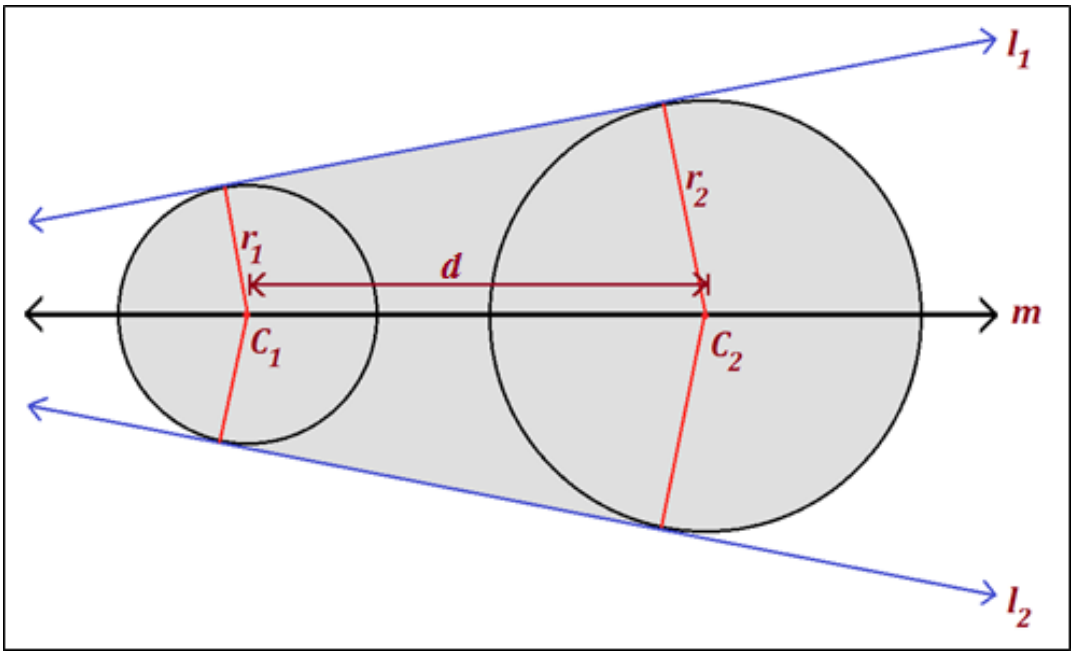

Figure 7. Illustration of the lopsided "Twinkie" shape. Two circles with centers C_1 and C_2 and radii r_1 and r_2 separated by a distance, *d*, along axis *m*. The shape of the initial vorticity field is the shaded portion bounded by the circles and their tangent lines, l_1 and l_2. Similar to other disturbances, a cubic-Hermite polynomial is used to gradually weaken the strength of the vorticity over a predetermined distance..

all six cases.

Case 1: Infinite Strip

Based on linear stability theory for an infinite strip of uniform vorticity, the wavelength of the most unstable mode is approximately eight times the width of the strip (Rayleigh, 1945; Guinn and Schubert, 1993). For uniform, infinite strips of width 200km, 300km and 400km, linear theory therefore predicts the strip to breakdown into approximately 4, 2.66 and 2 disturbances, respectively, when viewed over the model domain length of 6,400km. However, as described earlier, the infinite strips of vorticity are not uniform in the y direction because they smoothly taper at the edges. However, a uniform infinite strip of width 300 km would produce identical area-average vorticity to the infinite strip presented in cases 1-4. It is therefore reasonable to expect two to three disturbances to develop. The simulation verified this with three disturbances forming and developing as shown in Fig. 8. The evolution of the PV is very similar to Guinn and Schubert (1993).

Case 2: Infinite Strip with Uniformly Spaced Perturbations

In spite of the higher pockets of vorticity embedded along the infinite strip, there was little difference in the evolution of the PV from case 1. The circular regions of higher PV are quickly sheared into a single, relatively uniform strip, and the evolution then became nearly identical to that of case 1 as shown in Fig. 9. In fact, we noted in trial simulations (not shown) that the breakdown of the strip was more sensitive to the random phase shifts in the broadband perturbation than the magnitude of the circular regions of higher vorticity.

Case 3: Infinite Strip with Randomly Spaced Perturbations

As with case 2, the pockets of PV were quickly sheared; however, the resulting shape after shearing contained minor undulations as seen in Fig. 10. This resulted in the production of four disturbances rather than three as with previous case. However, we noted in simulations with longer run times, that two of the disturbances eventually merge leaving a total of three disturbances. The initial stages of merging can be seen the last panel of Fig. 10. In this panel, we see the third disturbance from the left is highly sheared and unable to develop, and it eventually merges with the neighboring disturbance to the left (not shown). The end result is the random spacing of the vorticity perturbations did little to alter the final pattern of disturbance; however, more time was required to reach the final state of three disturbances.

Case 4: Infinite Strip with Random Spaced Pockets of Convection

Despite the use of a mass sink instead of an initial

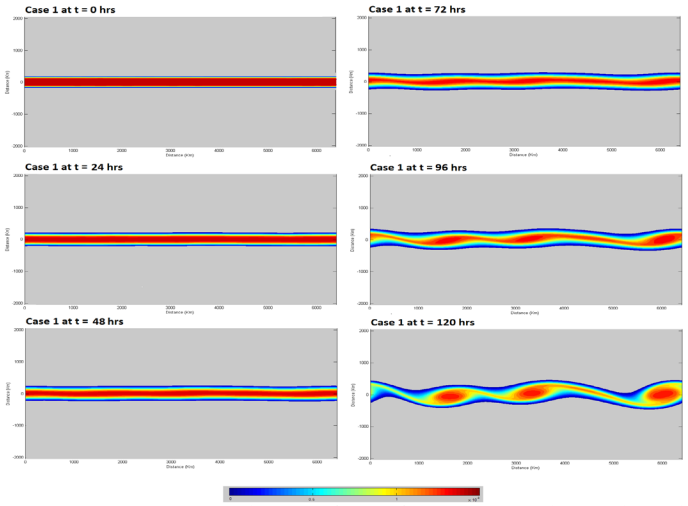

Figure 8. Case 1: PV evolution of an infinite strip 400km wide with a wavenumber 16 broadband perturbation.

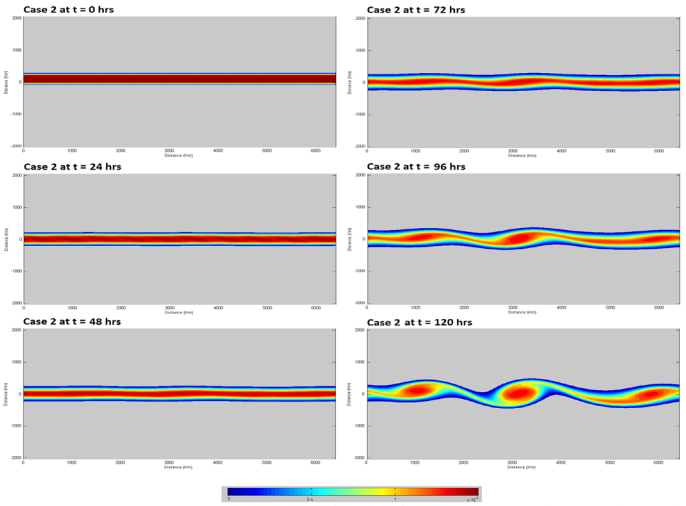

Figure 9. Case 2: PV evolution of an infinite strip 400km wide with 10 circular uniform spacing regions of higher PV embedded along the center of the strip.

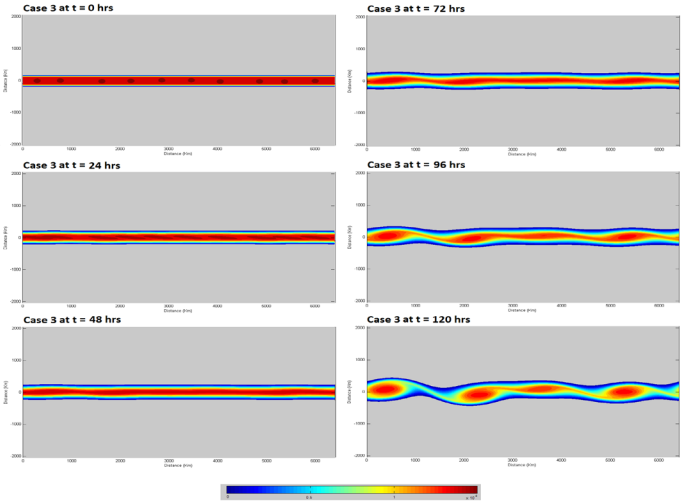

Figure 10. Case 3: PV evolution of an infinite strip 400km wide with 10 circular randomly spaced regions of higher PV embedded near the center of the strip.

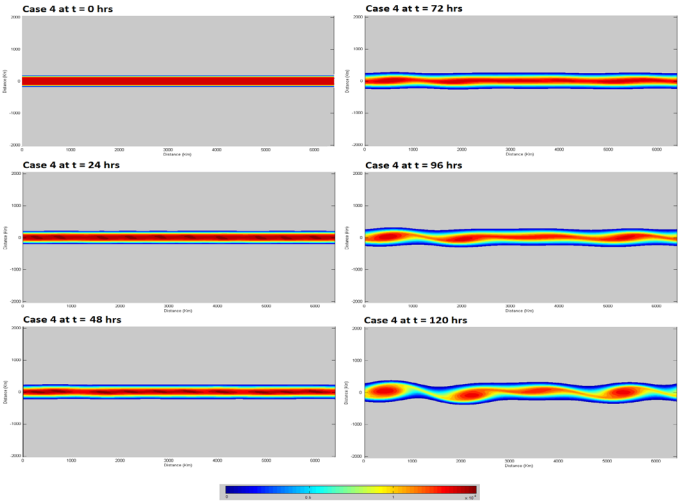

Figure 11. Case 4: PV evolution of an infinite strip 400km wide with 10 circular uniformly spaced mass sinks along the center of the strip.

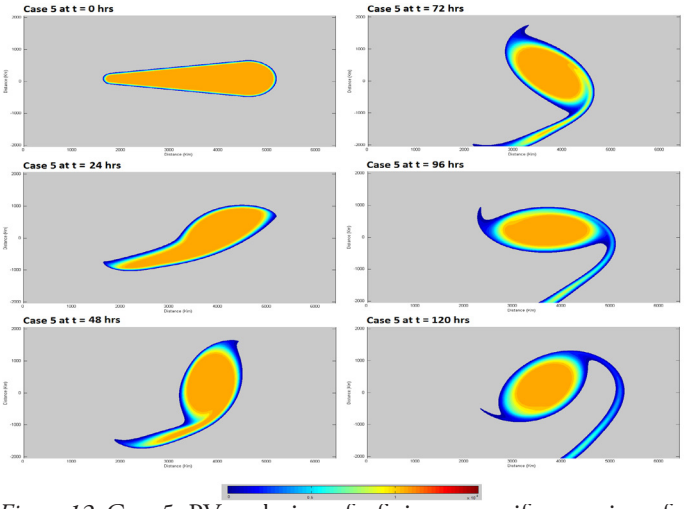

Figure 12. Case 5: PV evolution of a finite non-uniform region of vorticity.

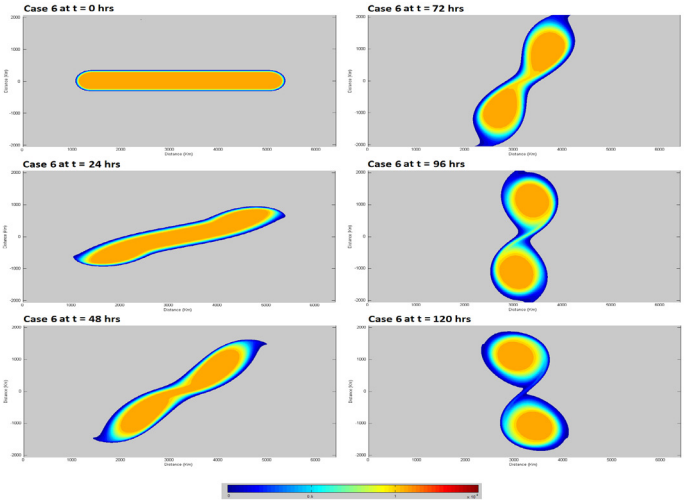

Figure 13. Case 6: PV evolution of a finite uniform region of vorticity (Twinkie shape).

vorticity perturbation and the lack of a broadband perturbation, the evolution of the strip was remarkably similar to case 3. This suggests the random placement of disturbances and the resulting undulations they create have a greater influence on the flow evolution than the broadband perturbation we used in the simulation (see Fig. 11).

Case 5: Unsymmetrical, Finite-Length Strip

This case differs from the others in that the initial vorticity disturbance is not infinite in the *x* direction. Thus, the circulation at the ends longitudinal ends of the PV strip can freely rotate the disturbance. The region with the larger pool of vorticity (eastern portion) has a much stronger resulting wind circulation and is initially pushed north. Later the disturbance shears the tail end of the disturbance leaving a spiral shaped band. These results are similar to those of Guinn and Schubert (1993) during the merger of two vortices. The lopsided PV shape, while not exact, is suggestive of the breakdown of the ITCZ and subsequent formation of TCs observed in the eastern Pacific. However, large displacements in the *y* direction make the *f*-plane approximation less valid in these simulations. Regardless, similar to the satellite time lapse (Fig. 6), the simulation in Fig. 12 also shows a thin tapering spiral band of PV extending from the center of circulation with little movement. This case may suggest barotropic processes are important in the evolution and breakdown of the ITCZ.

Case 6: Symmetrical, Finite-Length Strip

The breakdown of the finite strip is similar to Vaughan and Guinn (2013) for the same length to width ratio. The symmetry of the shape results in the same cyclonic wind circulation at both ends of the disturbance. Thus the shape rotates cyclonically at the same speeds on both sides of the disturbance. The strip eventually breaks down into two pools of uniform vorticity. It is interesting to note for comparison that for all variations in size and intensity for case 5 (lopsided strips), we did not observe a split as observed in Fig. 13. By noting the difference in evolution between case 5 and 6, we can conclude the initial shape of the finite strip plays a key role in determining the resulting PV evolution and merger. In addition, while not conclusive, the results suggest the splitting of a finite region of convection into two TCs is less likely if the initial convection is relatively asymmetric in shape.

Summary and Conclusions

The purpose of this paper was to expand previous work involving the use of simple barotropic models (Guinn and Schubert, 1993; Nieto-Ferreira and Schubert, 1997; Wang and Magnusdottir, 2005) in the study of ITCZ breakdown. Specifically, our first goal was to investigate the effect of simulated pockets of perturbation vorticity centers embedded within otherwise uniform strips of PV representing the ITCZ on the barotropic instability of the ITCZ. For initial conditions we specified the initial vorticity field then used the non-linear balance equation to determine the corresponding wind and mass fields. We then ran the model for a simulated 12 hrs in each case to observe the evolution of the PV field. These pockets of higher vorticity were intended to approximate the random pockets of intense convection observed in the actual ITCZ. While, the connection between convection and PV is only suggestive, it appears to produce similar results to the observed ITCZ evolution in many cases. Our second goal, was to investigate the evolution of irregularly shaped initial vorticity patterns of finite length. These represented the climatologically persistent irregularly shaped convective patterns found in the eastern Pacific Ocean. Lastly, we wanted to create a simple numerical model that could be used at the advanced undergraduate or introductory graduate level.

The experiments with the infinite strips showed there was limited sensitivity of the final PV pattern to the addition of uniformly spaced vorticity perturbations. These simulations tended to produce nearly identical solutions to the case without perturbations but with similar values of area-averaged vorticity. The perturbation areas were quickly sheared and the vorticity became uniformly distributed within the strip, leading to a nearly identical evolution. Results suggest the broadband perturbation played a bigger role in the final shape than the addition of vorticity pockets. However, when the perturbations given random offsets of ±25km in the direction *x* and ±200km in the *y* direction, the results tended to be slightly different compared to cases using the uniformly spaced perturbations. We believe the displacement in the *x* direction was the dominating effect because it effectively altered the initial wave pattern far more than the magnitude of the broadband perturbation. However, more work is needed for verification. We also examined the use of randomly spaced mass sinks to generate local regions of PV rather than specifying the perturbations initially. For this case, we turned off the broadband

perturbation. We noticed from the results that the random spacing of the perturbations again tended to have a dominate effect on the evolution of the PV field. Thus, these last two cases produced nearly identical results, generating a wavenumber four pattern compared to wavenumber three pattern in the previous two cases. We also noted that when the simulation was extended for longer periods of time, two of the disturbances merged to create a wavenumber three pattern as predicted by linear stability theory. We conclude that the final shape for this case closely matches that predicted by linear stability theory.

In the second set of experiments, we examined irregularly shaped PV patterns of finite length. Here we wanted to expand the studies of Vaughan and Guinn (2013) by comparing the evolution of symmetric patterns with non-symmetric patterns. The asymmetry led to significantly different evolutions in the PV field. Most notably the asymmetric pattern never separated into two distinct vorticity patterns. While not conclusive, this suggests that in nature the development of two TCs from a region of enhanced convection may be difficult if the initial region of convection is not relatively symmetric to start.

Lastly, one of the objectives of this project was to develop a normal-mode spectral model in a user-friendly programming language that can be used for both education and research at the undergraduate and introductory level. The fast Fourier transforms and matrix manipulation algorithms in MATLAB® made it an ideal choice for this research project and future research work. The normal-mode technique also allows the user to separate the rotational (Rossby) modes from the gravitational modes (Guinn and Schubert, 1993), although this capability was not used in this current research, it may be beneficial for other studies. Lastly, it is noteworthy to mention the following quote by S. G. H. Philander et al. (1996).

> *"The most complex models are capable of the greatest realism, but their results are difficult to analyze and explain. It is therefore important to have simpler models that by excluding certain processes, sacrifice realism, but in return allow detailed analysis and yield physical insight into the retained processes"*

While the normal mode barotropic model with an *f*-plane approximation is unable to serve as a reliable forecasting tool, simple barotropic models such as these still offer excellent insight from a theoretical standpoint, and they are still relevant to gaining insight into TC dynamics (*e.g.* Hendricks et.al, 2014). Please contact the author if you are interested in obtaining a copy of the MATLAB® scripts used for this project.

References

DeMaria, M., and Schubert W. H., 1984: Experiments with a Spectral Tropical Cyclone Model. *J. Atmos. Sci.*, **41**, 901–924. doi: http://dx.doi.org/10.1175/1520-0469(1984)041<0901:EWASTC>2.0.CO;2

Gray, W. M., 1979: Hurricanes: Their formation, structure and likely role in the tropical circulation. *Meteorology over the Tropical Oceans*, D. B. Shaw, Ed., *Roy. Meteor. Soc.*, 155–218. doi: 10.1002/qj.49710644918

Guinn, T. A., 1992: A dynamical theory for hurricane spiral bands. Ph.D. dissertation, Dept. of Atmospheric Science, Colorado State University, 178 pp.

Guinn, T. A., and Schubert W. H., 1993: Hurricane spiral bands. *J. Atmos. Sci.*, **50**, 3380–3403. doi: http://dx.doi.org/10.1175/1520-0469(1993)050<3380:HSB>2.0.CO;2

Hendricks, E. A., W. H. Schubert, Y.-H. Chen, H.-C. Kuo, and M. S. Peng (2014), Hurricane eyewall evolution in a forced shallow water model, *J. Atmos. Sci.*, **71**, 1623–1643. doi: http://dx.doi.org/10.1175/JAS-D-13-0303.1

Mattuck, A., M., H. Miller, J. Orloff, and J. Lewis. 18.03SC Differential Equations, Fall 2011. (Massachusetts Institute of Technology: MIT OpenCourseWare Available online at http://ocw.mit.edu.).

Nieto-Ferreira, R., and Schubert W. H., 1997: Barotropic aspects of ITCZ breakdown. *J. Atmos. Sci.*, **54**, 261–285.

Philander, S. G. H., D. Gu, G. Lambert, T. Li, D. Halpern, N-C. Lau, and R. C. Pacanowski, 1996: Why the ITCZ Is Mostly North of the Equator. *J. Climate*, **9**, 2958–2972. doi: http://dx.doi.org/10.1175/1520-0469(1997)054<0261:BAOIB>2.0.CO;2

Rayleigh, J. W. S., 1945: Vortex Motion and Sensitive Jets, The Theory of Sound, Vol 2, *Dover Publications*, 376-414.

Salby, M. L., Hendon, H. H., Woodberry, K, and Tanaka, K, 1991: Analysis of Global Cloud Imagery from Multiple Satellites. *Bull. Amer. Meteor. Soc.*, **72**, 467–480. doi: http://dx.doi.org/10.1175/1520-0477(1991)072<0467:AOGCIF>2.0.CO;2

Schubert, W. H., M. T. Montgomery, R. K. Taft, T. A. Guinn, S. R. Fulton, J. P. Kossin, J. P. Edwards, 1999: Polygonal eyewalls, asymmetric eye contraction, and potential vorticity mixing in hurricanes. *J. Atmos. Sci.*, **56**, 1197-1223. doi: http://dx.doi.org/10.1175/1520-0469(1999)056<1197:PEAECA>2.0.CO;2

Thelwell, R, 2001: The Nonlinear Balance Equation: a Survey of Numerical Methods. Master's Thesis, Colorado State University.

Vaughan, M. T and Guinn, T. A., 2013: The Evolution of Finite Vorticity Strips using a Non-Divergent Barotropic Model. 12th Annual Student Conference, Austin, TX, Amer. Meteor. Soc., S68. [Available online at *https://ams.confex.com/ams/93Annual/webprogram/Paper224776.html.*]

Wang, C. and Magnusdottir, G., 2005: ITCZ Breakdown in Three-Dimensional Flows. *J. Atmos. Sci.*, **62**, 1497–1512. doi: http://dx.doi.org/10.1175/JAS3409.1

Waliser, D. E., and Gautier, C, 1993: A Satellite-derived Climatology of the ITCZ. *J. Climate*, **6**, 2162–2174. doi: http://dx.doi.org/10.1175/1520-0442(1993)006<2162:ASDCOT>2.0.CO;2

Authors

Ajay Raghavendra

Ajay recently graduated from Embry-Riddle Aero. Univ., Daytona Beach, FL with a B.S. in Meteorology and a B.S. in Computational Mathematics (Magna Cum Laude and Honors Program). He is currently pursuing his Ph.D. in Atmospheric Science at the University of Albany (SUNY), NY. As an undergraduate student, Ajay fueled his thirst for knowledge by conducting research in tropical meteorology and fluid dynamics. Thanks to the generous mentorship by his professors (including the research work presented in this paper), Ajay completed independent research projects in the climatology of tropical cyclones (TC) climatology (Dr. R.J. Barry), the dynamics of the Inter-Tropical Convergence Zone (Dr. T.A. Guinn), the transition of extratropical TCs (Dr. S. M. Milrad) and the evolution of polygonal shapes in Leidenfrost Drops (Dr. A. Ludu). He has presented his works in professional conferences, manuscripts and a book chapter.

Dr. Thomas Guinn

Thomas Guinn is an Associate Professor of Meteorology and the Coordinator for both the B.S. in Meteorology and B.S. in Operational Meteorology programs at Embry-Riddle Aeronautical University in Daytona Beach, Florida. He joined the Embry-Riddle faculty in 2008 after completing a 22-year career in the U.S. Air Force as a weather officer. Dr. Guinn received a B.S. in Meteorology from Iowa State University (1985) as well as an M.S. (1989) and Ph.D. (1992) in Atmospheric Science from Colorado State University. Dr. Guinn has taught graduate and undergraduate courses in aviation meteorology as well as undergraduate courses in synoptic meteorology, mesoscale meteorology, dynamic meteorology, and numerical weather prediction. In addition to tropical cyclone dynamics, his research interests include aviation meteorology and aviation weather education. Dr. Guinn serves on the American Meteorological Society's Board on Higher Education.